

Phase diagram and critical behavior of the square-lattice Ising model with competing nearest- and next-nearest-neighbor interactions

Junqi Yin and D. P. Landau
*Center for Simulational Physics, University of Georgia,
 Athens, Georgia 30602, USA*

(Dated: May 29, 2018)

Using the parallel tempering algorithm and GPU accelerated techniques, we have performed large-scale Monte Carlo simulations of the Ising model on a square lattice with antiferromagnetic (repulsive) nearest-neighbor (NN) and next-nearest-neighbor (NNN) interactions of the same strength and subject to a uniform magnetic field. Both transitions from the (2×1) and row-shifted (2×2) ordered phases to the paramagnetic phase are continuous. From our data analysis, reentrance behavior of the (2×1) critical line and a bicritical point which separates the two ordered phases at $T=0$ are confirmed. Based on the critical exponents we obtained along the phase boundary, Suzuki's weak universality seems to hold.

PACS numbers: 75.40.Mg, 64.60.De, 64.60.F-

I. INTRODUCTION

For the nearest-neighbor (NN) Ising antiferromagnet on the square lattice in a uniform magnetic field, the low temperature ordered phase is separated from the paramagnetic phase by a simple, 2nd order phase boundary. (Within the context of the lattice gas model this system could be described as having repulsive NN-coupling and forming a $c(2 \times 2)$ ordered state.) With the addition of repulsive (antiferromagnetic) next-nearest-neighbor (NNN) interactions the situation becomes more complicated. Early Monte Carlo simulations suggested that a single, super-antiferromagnetic, or (2×1) , phase existed, separated from the paramagnetic phase by a single phase boundary[3, 4, 5]. A degenerate, row-shifted (2×2) state was also predicted at zero temperature. (See Fig. 1 for a schematic representation of these states.) On the other hand, symmetry arguments based on Landau theory[1] predict the order-disorder transitions of (2×1) and (2×2) structures belong to XY model with cubic anisotropy.

The original motivation of this study was to investigate the possibility of XY-like behavior of the Ising spins on the square lattice, since there is numerical evidence[2] that Ising antiferromagnet with attractive NNN interaction on the triangular lattice has an XY-like intermediate state between the low temperature ordered state and high temperature disordered state. In fact, the present model has already been studied by many authors using different approaches. An early Monte Carlo study[5] comprehensively showed the phase diagrams for several different interaction ratios (R) of NNN to NN interaction. But due to the deficiencies of computer resources at that time, for the $R = 1$ case, a disordered region was missed between the two ordered phases which was pointed out in a later interfacial free energy study[6]. Meanwhile, transfer matrix studies[7, 8] found reentrant behavior for the (2×1) transition lines. While a study using the clus-

ter variation method[9, 10] concluded that for a range of R ($0.5 \sim 1.2$) the system undergoes a first order transition, a recent Monte Carlo study[11] using a variant of the Wang-Landau method[12] focused on the $R = 1$ case without external field and found the phase transition is of second order. For external field $H = 4$ (in the unit of NN interaction constant) the two ordered phases, namely (2×1) and row-shifted (2×2) , are degenerate at zero temperature so it is tempting to think that the cubic anisotropy would be zero for this field and that there could be a Kosterlitz-Thouless transition.

In this paper, we carefully study the location of phase boundaries and the critical behavior for the case $R = 1$. In Sec. II the model and relevant methods and analysis techniques are reviewed. Our results are presented in Sec. III, along with finite size scaling analyses, and we summarize and conclude in Sec. IV.

II. MODEL AND METHOD

A. The model

The Ising model with NNN interaction is described by the Hamiltonian

$$\mathcal{H} = J_{NN} \sum_{\langle i,j \rangle_{NN}} \sigma_i \sigma_j + J_{NNN} \sum_{\langle i,j \rangle_{NNN}} \sigma_i \sigma_j + H \sum \sigma_i, \quad (1)$$

where $\sigma_i, \sigma_j = \pm 1$, J_{NN} and J_{NNN} are NN and NNN interaction constants, respectively, H is an external magnetic field, and the sums in the first two terms run over indicated pairs of neighbors on a square lattice with periodic boundary conditions. Both J_{NN} and J_{NNN} are positive (antiferromagnetic) and the ratio $R = J_{NNN}/J_{NN}$.

For the $R = 1$ case, the ground states would be the (2×1) state, also known as super-antiferromagnetic state, in small magnetic fields; and at higher fields it would be a row-shifted (2×2) state, which differs from the (2×2)

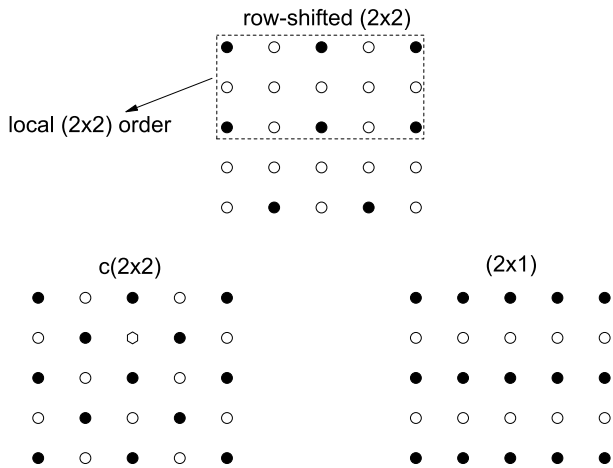


FIG. 1: Schematic plots of $c(2 \times 2)$, (2×1) and row-shifted (2×2) ordered structures within the context of the lattice gas model. (In magnetic language, filled circles correspond to up spins and empty circles correspond to down spins.)

state in the sense that the antiferromagnetic chains in the former state can slide freely without energy cost. See Fig. 1. Locally, the structure may appear to be (2×2) , but for large enough lattices the equilibrium structure always shows row shifting. As a result, such a row-shifted (2×2) state is highly degenerate, and the antiferromagnetic sublattice exhibits only one dimensional long range order. In terms of the sublattice magnetizations

$$M_\lambda = \frac{4}{N} \sum_{i \in \lambda} \sigma_i, \quad \lambda = 1, 2, 3, 4 \quad (2)$$

we can define two components of the order parameter for the (2×1) state

$$M^a = [M_1 + M_2 - (M_3 + M_4)]/4, \quad (3)$$

$$M^b = [M_1 + M_4 - (M_2 + M_3)]/4, \quad (4)$$

with a computationally convenient root-mean-square order parameter

$$M^{rms} = \sqrt{(M^a)^2 + (M^b)^2}. \quad (5)$$

Since M^{rms} would have a limiting value of $\frac{1}{2}$ for the row-shifted (2×2) state and be zero for the disordered state, it can also be used as an order parameter for the row-shifted (2×2) state.

Other observables, such as the finite lattice ordering susceptibility χ and fourth-order cumulant U , are defined in terms of the order parameter M^{rms} as

$$\chi = \frac{N}{T} [\langle (M^{rms})^2 \rangle - \langle M^{rms} \rangle^2] \quad (6)$$

$$U = 1 - \frac{\langle (M^{rms})^4 \rangle}{3 \langle (M^{rms})^2 \rangle^2} \quad (7)$$

where N is the total number of spins and T is the simulation temperature. In some cases, the true ordering susceptibility χ^+ , which is $\frac{N}{T} \langle (M^{rms})^2 \rangle$, is used to eliminate simulation errors resulting from $\langle M^{rms} \rangle$, where the order parameter is known to be zero for the infinite lattice.

B. Simulation methods

For small lattice sizes, Wang-Landau sampling [12] was used to obtain a quick overview of the thermodynamic behavior of our model. A two-dimensional random walk in energy and magnetization space was performed so that the density of states $g(E, M)$ could be used to determine all thermodynamic quantities (derived from the partition function) for any value of temperatures and external field. Consequently, "freezing" problems are avoided at extremely low temperatures. This allowed us to determine the "interesting" regions of field-temperature space; however, it quickly became apparent that, because of subtle finite size effects, quite large lattices would be needed. Unfortunately, as L increases, the number of entries of histogram explodes as L^4 and it proved to be more efficient to use parallel tempering instead.

Since a large portion of interesting phase boundary is at relatively low temperatures and many local energy minima exist which makes the relaxation time rather long, the parallel tempering method [13, 14] is a good choice for simulating our model. The basic idea is to expand the low temperature phase space by introducing configurations from the high temperatures. So, many replicas at different temperatures are simulated simultaneously, and after every fixed number of Monte Carlo steps, a swap trial is performed with a Metropolis-like probability which satisfies the detailed balance condition. The transition probability from a configuration X_m simulated at temperature β_m to a configuration X_n simulated at temperature β_n would be

$$W(X_m, \beta_m | X_n, \beta_n) = \min[1, \exp(-\Delta)], \quad (8)$$

$$\Delta = (\beta_n - \beta_m)(\mathcal{H}_m - \mathcal{H}_n). \quad (9)$$

We chose the temperatures for the replicas to be in a geometric progression [15], which would make acceptance rates relatively constant among neighboring temperature pairs, and the total number of temperatures was chosen to make the average acceptance rate above 20%.

The multiplicative, congruential random number generator RANECU was used [16, 17], and some results were also obtained using the Mersenne Twister [18] for comparison. No difference was observed to within the error bars.

Typically, data from 10^6 to 10^7 MCS were kept for each run and 3 to 6 independent runs are taken to calculate standard statistical error bars. For parallel tempering, the swap trial was attempted after every MCS. In all the

plots of data and analysis shown in following sections, if error bars are not shown they are always smaller than the size of the symbols.

In general, such replica exchange not only applies to the temperature set, but also can apply to any other sets of fields, such as the external magnetic field. Following the same argument, one can get the transition probability from $\{X_m, H_m\}$ to $\{X_n, H_n\}$

$$W(X_m, H_m | X_n, H_n) = \min[1, \exp(-\Delta)], \quad (10)$$

$$\Delta = \beta(H_n - H_m)(M_m - M_n). \quad (11)$$

where M_m, M_n are the uniform magnetizations of replica m and n , respectively.

C. Finite-size scaling analysis

To extract critical exponents from the data, we performed finite-size scaling analyses along the transition lines. Since the maximum slope of the fourth-order cumulant U follows[19]

$$\left(\frac{dU}{dK}\right)_{max} = a' L^{\frac{1}{\nu}} (1 + b' L^{-\omega}), \quad (12)$$

where $K = \frac{J_{NN}}{k_B T}$, the correlation length exponent ν can be estimated directly.

With the exponent ν and critical temperature T_c at hand, the critical exponent β and γ can be extracted from the data collapsing of the finite-size scaling forms,

$$M = L^{-\frac{\beta}{\nu}} \bar{X}(tL^{\frac{1}{\nu}}) \quad (13)$$

$$\chi T = L^{\frac{\gamma}{\nu}} \bar{Y}(tL^{\frac{1}{\nu}}) \quad (14)$$

where $t = |1 - \frac{T}{T_c}|$, and \bar{X} and \bar{Y} are universal functions whose analytical forms are not known. One can also estimate the exponent α from the relation of the peak position with lattice size for the specific heat

$$C_{max} = cL^{\frac{\alpha}{\nu}} + C_0 \quad (15)$$

where C_0 is the "background" contribution. In some cases when the appropriate paths, i.e. which are perpendicular to the phase boundary, are ones of constant temperatures, then the critical behavior would be expressed in terms of reduced field $h = |1 - \frac{H}{H_c}|$, and all the above analysis still applies.

D. GPU acceleration

General purpose computing on graphics processing units(GPU) attracts steadily increasing interest in simulational physics[20, 21, 22], since the computational

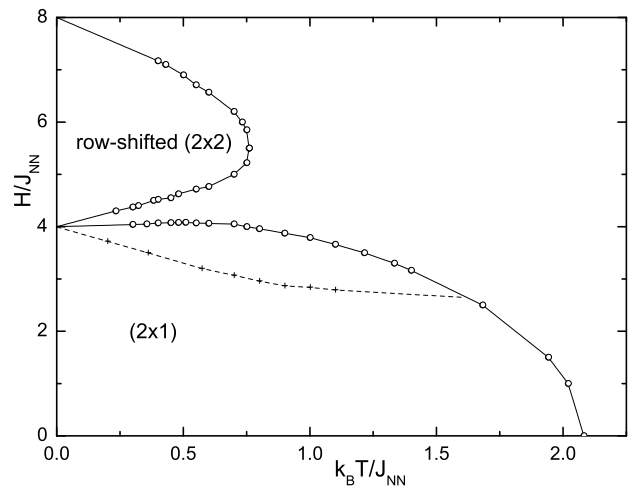


FIG. 2: The phase diagram for the Ising square lattice with antiferromagnetic nearest- and next-nearest-neighbor interactions in a magnetic field for $R = 1$. Open circles and pluses denote simulation results. The solid lines are second order transition lines, while the dashed line indicates the short range ordering line.

power of recent GPU exceeds that of a central processing unit(CPU) by orders of magnitude. The advantage continues to grow as the performance of GPU's doubles every year. Recently, a GPU accelerated Monte Carlo simulation of Ising models[22] was performed. Compared to traditional CPU calculations, the speedup was about 60 times.

The idea behind the implementation in Ref [22] can be easily extended to our model, and the parallel tempering algorithm is naturally realized. Initially, all the replica are loaded to the global memory of the GPU. For each replica, the entire lattice is divided into four sublattices, then spins in the same sublattice can be updated simultaneously by the GPU using a Metropolis scheme, and the swap of configurations of replica pairs can also be achieved in parallel.

On the GeForce GTX285 graphics unit, our code runs about 10 times faster than it does on the 32 CPUs of IBM p655 cluster using Message Passing Interface(MPI) for parallel computation.

III. RESULTS AND DISCUSSION

A. Phase diagram and short range ordering

From the ground state analysis, with zero or low field the ordered state would be the superantiferromagnetic, or (2×1) , structure. As the external field increases to $4 < H/J_{NN} < 8$, more spins align in the opposite field direction, and the ordered structure would be the row-shifted (2×2) . With even stronger fields, the system becomes paramagnetic. In the region near $H/J_{NN} = 4$

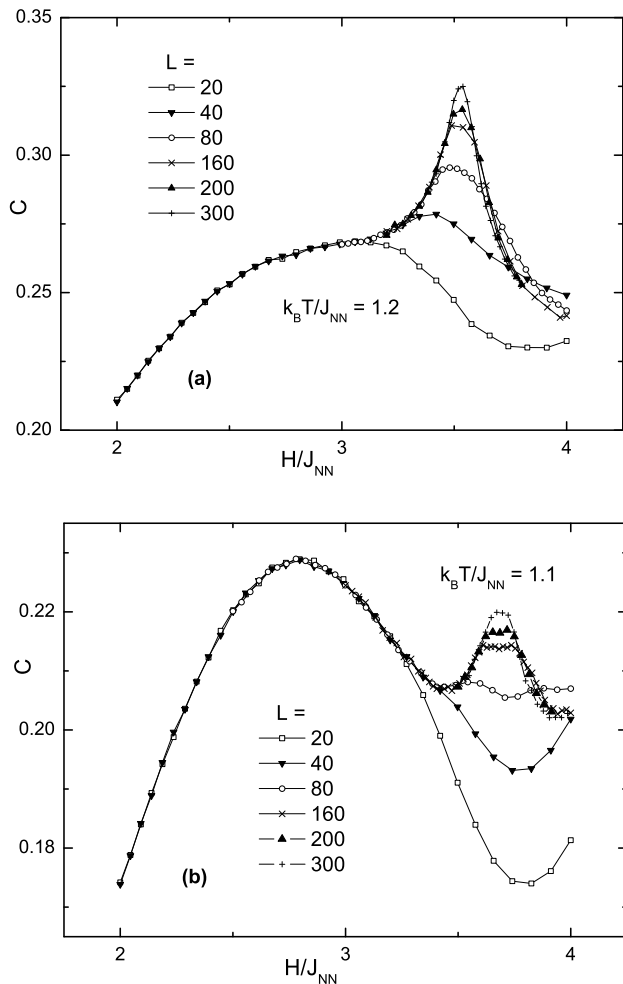


FIG. 3: Variation of the specific heat C versus field H with lattice sizes $L = 20, 40, 80, 160, 200, 300$ for paths of constant: (a) $k_B T / J_{NN} = 1.2$ and (b) $k_B T / J_{NN} = 1.1$.

a mixture of (2×1) and row-shifted (2×2) is visible.

For finite temperatures, we found that the fourth-order cumulant is always a good quantity to use to locate the transition points, while the data for other quantities, such as the specific heat or susceptibility, may look "strange" due to the effect of neighboring critical points. To help the reader understand the observed thermodynamic properties, the final phase diagram for $R = 1$ is plotted in Fig. 2: The solid lines are the phase boundaries, all of which are continuous. The dashed line inside the (2×1) ordered phase indicates a "short range ordering" line, which was located from the peak position of the specific heat. As shown in Fig. 3, for paths of constant temperature $k_B T / J_{NN} = 1.1$ and 1.2 , there are two peaks, and the one that increases with lattice size eventually corresponds to the critical point.

An indication of the complexity of the finite size behavior is clearly seen in the bottom portion of Fig. 3 in which the small lattices actually have minima in the specific heat for field values that eventually show phase tran-

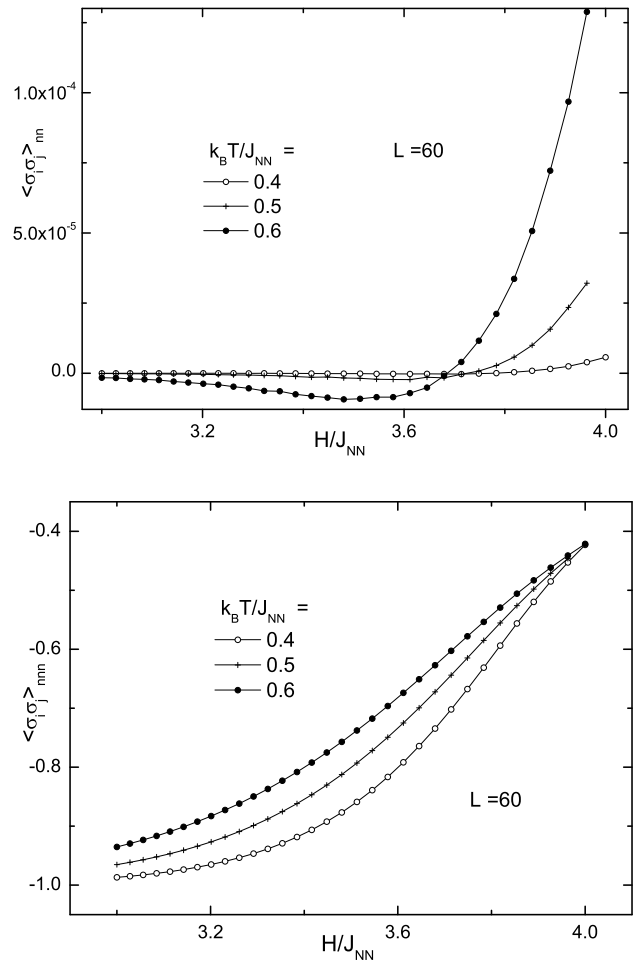


FIG. 4: Nearest- and next-nearest-neighbor correlation functions. The field is varied for paths of 3 different temperatures: $k_B T / J_{NN} = 0.4, 0.5$ and 0.6 across the short range ordering line.

sitions for sufficiently large systems. The round-shaped size-independent peak is due to the short range ordering of the (2×1) "clusters" of different orientation from the ordered background. No corresponding behavior was observed from the susceptibility or the fourth-order cumulant.

In order to confirm the above argument, we also calculated the NN and NNN pair correlation function, that is $\langle \sigma_i \sigma_j \rangle$, for paths of different fields crossing this line. The correlation function data are plotted in Fig. 4. The NN pair correlation decreases from zero to a minimum and then increases to positive values, while the NNN pair correlation increases monotonically from -1 .

B. Critical behavior

The data for the specific heat and susceptibility for three different values of H are plotted in Fig. 5.

Without the field, they both show very sharp peaks,

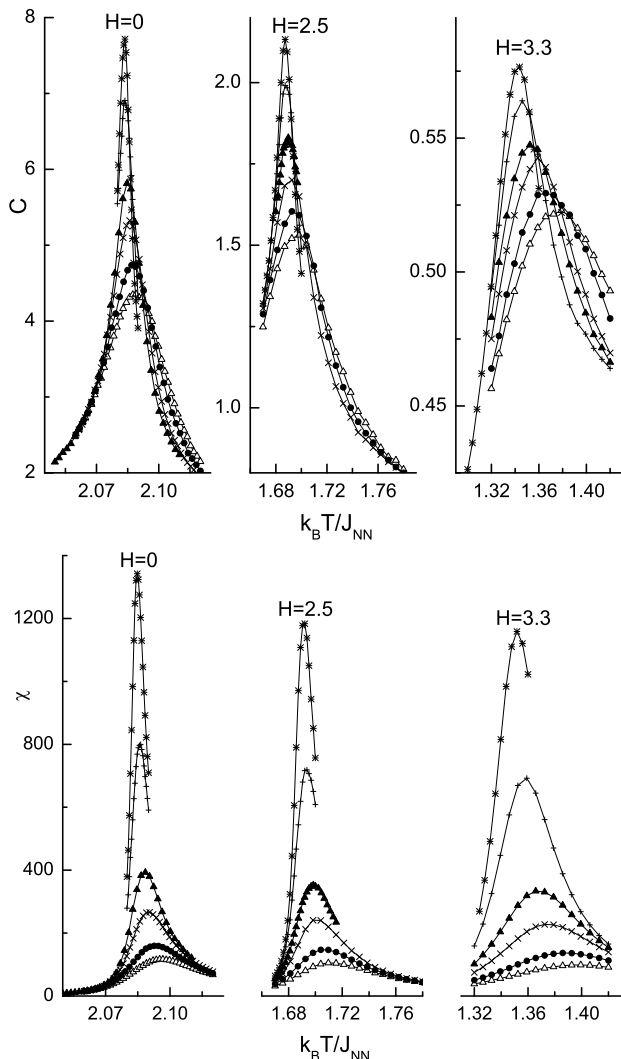


FIG. 5: Specific heat and susceptibility for 3 different fields across the phase boundary. Data are for: $L=100$, Δ ; $L=120$, \bullet ; $L=160$, \times ; $L=200$ \blacktriangle ; $L=300$ $+$; $L=400$ $*$.

and from the magnitudes of the peak values of the specific heat, as shown in Fig.6(b), we can obtain a rather accurate estimate of the exponent ratio $\alpha/\nu = 0.357(8)$, which is obviously not zero. In Fig.6(a), we also show the curve-fit for the maximum slope of $\frac{dU}{dK}$ for $H = 0$, and extract the exponent $\nu = 0.847(4)$ directly.

Both values of α and ν are quite consistent with the early estimates in ref [5], and the value of α/ν is different from ref [11], in which the $1/L$ correction term was assumed up to lattice size $L = 160$.

The same procedure was repeated for $H/J_{NN} = 2.5$ and 3.3 , however, as shown in Fig. 5, the peaks of the specific heat become increasingly rounded as the field increases, which makes it rather difficult to get a direct estimate of the exponent α . Because of this it was necessary to obtain data for much larger lattice sizes, a task that was only possible with the use of GPU computing. In fact, as the value of ν increases with the

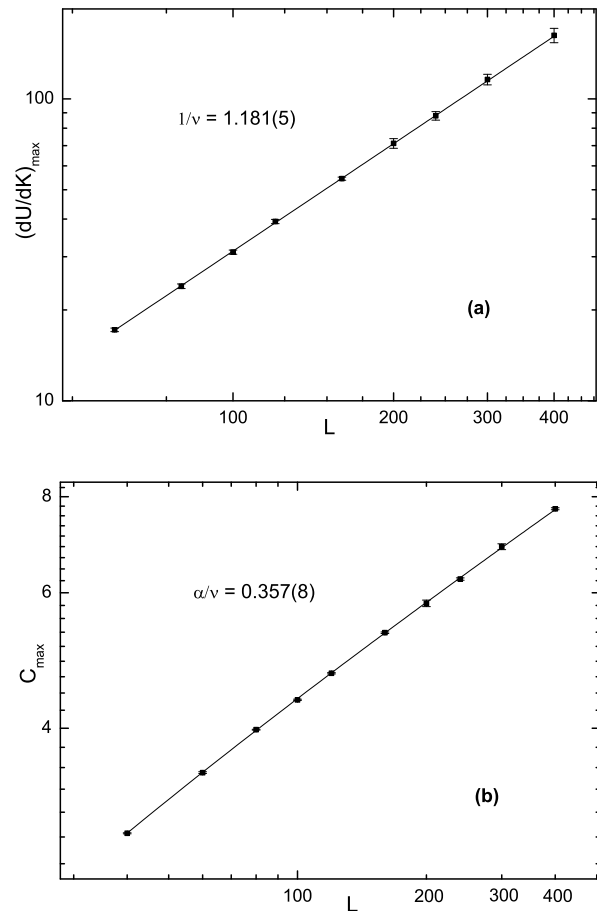


FIG. 6: Curve fits using the leading terms of equations 12 and 15 for the maximum slopes of $\frac{dU}{dK}$ (a) and peak values of specific heat (b), respectively.

field, for $H/J_{NN} = 3.3$, according the hyper-scaling law $\alpha = 2 - d\nu$, where $d = 2$ is the dimension of the system, α should be negative. Although the curve-fit is not stable, given the value of α we can get a fit within error bars. Such continuous increasing of the exponent ν up to values much greater than one is actually consistent with the findings of an early transfer-matrix study[8].

To estimate the critical exponents β and γ , we performed data collapsing with a large range of lattice sizes for the order parameter and its susceptibility. As shown in Fig. 7, the data in both finite size scaling plots collapse very nicely onto single curves, and the ratio β/ν and γ/ν agree with values of the 2D Ising universality class within error bars.

Hence, although the individual exponents are non-universal, Suzuki's weak universality holds quite well. Another data collapsing along the path of constant $H/J_{NN} = 6$ across the phase boundary of the row-shifted 2×2 state is shown in Fig. 8. The quality of the data collapsing is also excellent, and again, the exponents are non-universal. The estimate for β/ν is a bit low but γ/ν agrees well with prediction of weak universality.

In Table. I, the critical points and exponents α, β, ν

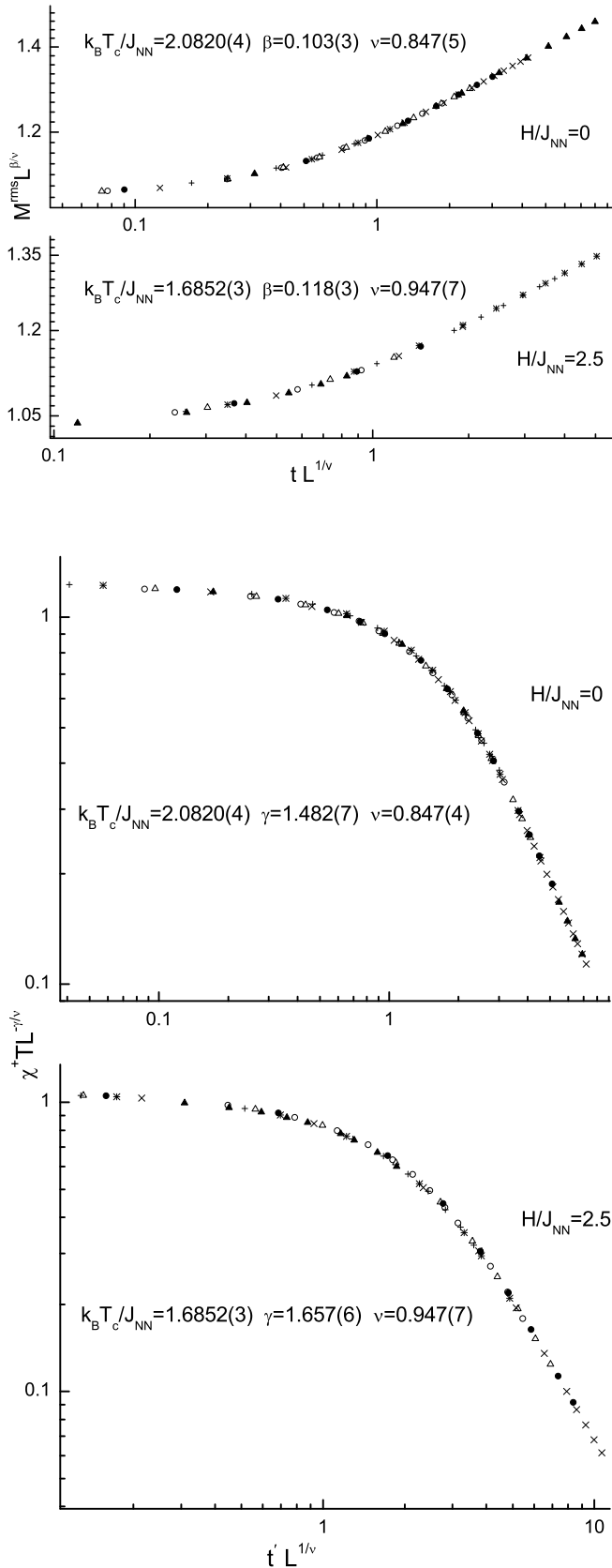


FIG. 7: Finite size scaling data collapsing along paths of constant $H/J_{NN} = 0$ and 2.5 for root-mean-square order parameter and its ordering susceptibility, respectively. $t' = |1 - \frac{T}{T_c}|$ and $t = (1 - \frac{T}{T_c})$. Data are for: $L=80$, \circ ; $L=100$, Δ ; $L=120$, \bullet ; $L=160$, \times ; $L=200$ \blacktriangle ; $L=300$, $+$; $L=400$, $*$.

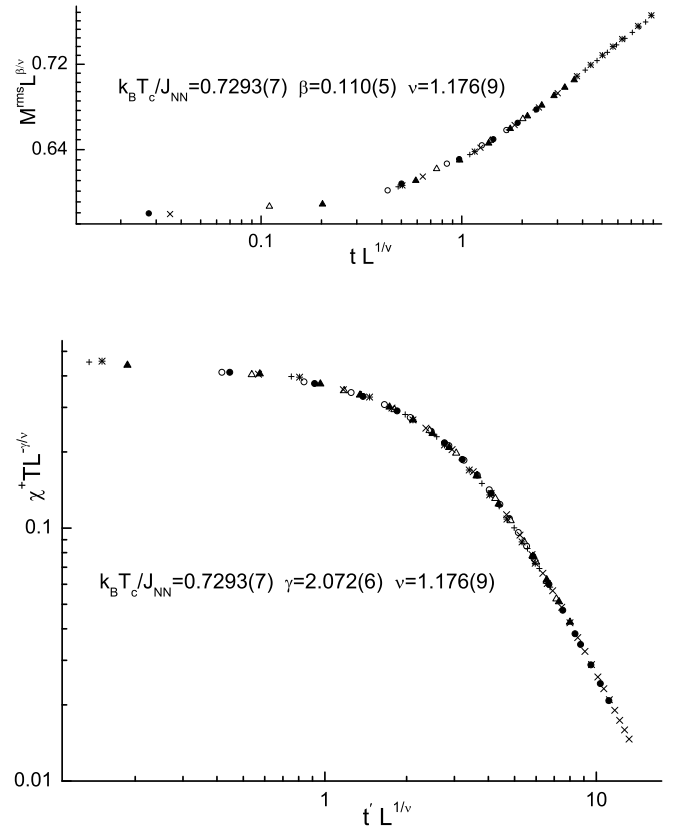


FIG. 8: Data collapsing along the path of constant $H/J_{NN} = 6$ for root-mean-square order parameter and its ordering susceptibility, respectively. Data are for: $L=80$, \circ ; $L=100$, Δ ; $L=120$, \bullet ; $L=160$, \times ; $L=200$ \blacktriangle ; $L=300$, $+$; $L=400$, $*$.

order	path	T_c or H_c	α	β	γ	ν
	$H=0$	2.0820(4)	0.302(7)	0.103(3)	1.482(7)	0.847(4)
2×1	$H=2.5$	1.6852(3)	0.104(19)	0.118(3)	1.657(6)	0.947(7)
	$H=3.3$	1.3335(6)		0.130(5)	1.930(6)	1.102(8)
$2 \times 2^*$	$H=6$	0.7293(7)		0.110(5)	2.072(6)	1.176(9)
	$T=0.5$	6.848(5)		0.126(4)	1.775(5)	1.02(2)

TABLE I: Values of critical point temperatures or magnetic fields and corresponding critical exponents for several paths of constant temperature or field across the phase boundary of the (2×1) and $2 \times 2^*$ row-shifted (2×2) ordered phases.

and γ for several typical paths of constant H or T across the phase boundary are listed.

C. Reentrance behavior

Close to the region between the two ordered phases the correlation length exponent ν turns out to be quite large, and correspondingly the location of the critical points becomes very difficult to determine. In addition, the

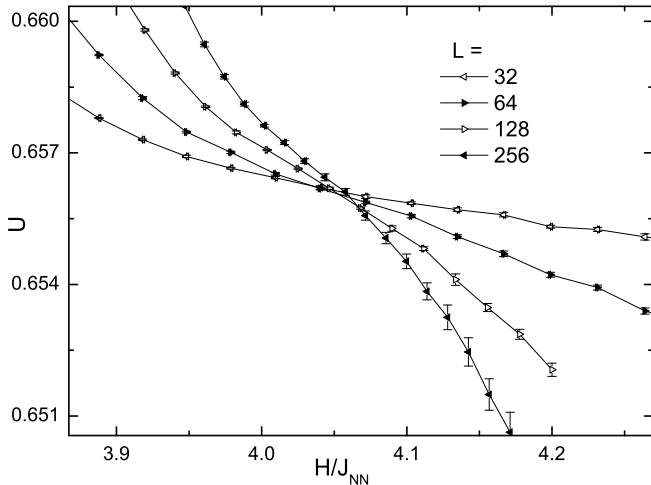


FIG. 9: Fourth order cumulant U versus field H along the path of constant $k_B T/J_{NN} = 0.7$ for lattice size $L = 32, 64, 128, 256$.

specific heat curves look "strange", see Fig. 3, because the exponent α/ν would have a negative value with large magnitude, much larger lattice size is needed to approach to the limiting peak value. Since Suzuki's weak universality seems to hold along the transition line, we fixed the values of $\beta/\nu = 0.125$ and $\gamma/\nu = 1.75$ for the data collapsing analysis to get a better estimate of the critical point and the exponent ν .

As shown in Fig. 9, the crossing point of the fourth order cumulant curves for a path of constant $k_B T/J_{NN} = 0.7$ is slightly above $H/J_{NN} = 4$, and from the data collapsing analysis, see Fig. 10, we obtained an estimate of the critical point to be $H_c/J_{NN} = 4.052(7)$. Hence, we confirm the reentrant behavior of the (2×1) transition line.

For the paths of constant $k_B T/J_{NN} = 0.45$, the curves of the fourth order cumulant shows two crossing points and the finite size effect is quite obvious. See Fig. 11.

For the larger lattice size, the two crossing points move towards lower fields but they do not approach each other. Thus, a region of disorder remains between the two different ordered states, even down to quite low temperatures. (If however, small lattices are used with insufficient data precision, it looks as though the curves for different lattice sizes coincide. Such behavior would indicate, erroneously, the presence of an XY-like region.) In Fig. 12, we show data collapsing fits along the path of constant $k_B T/J_{NN} = 0.5$ (and excellent data collapsing is also found along the path of constant $k_B T/J_{NN} = 0.3$), which confirms that there is a disordered region in between the two ordered states.

We thus conclude that there is no XY-like region and that the two phase boundaries probably only come together at a bicritical point at $T = 0$, although we cannot exclude the possibility of a bicritical point at very low, but non-zero, temperature. However, the data do

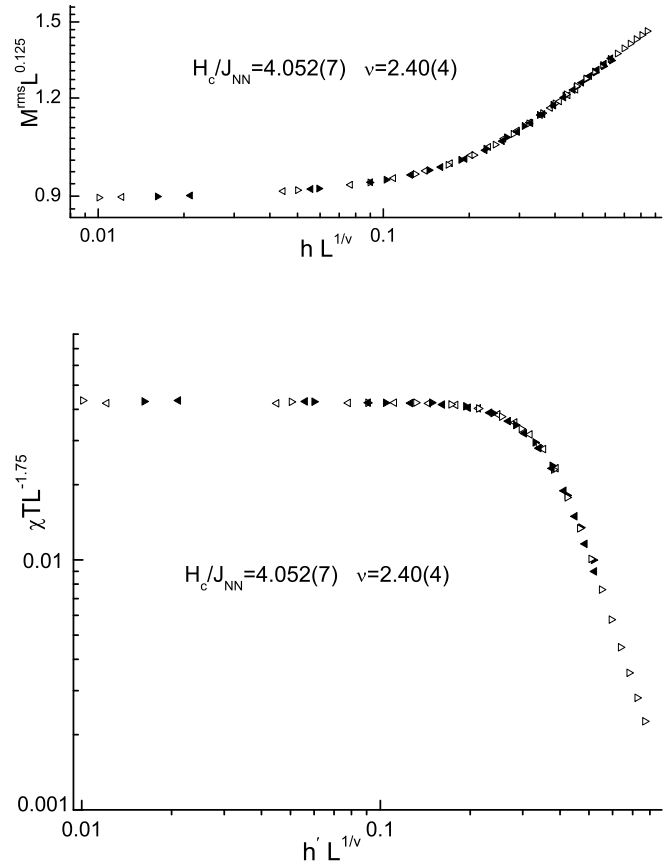


FIG. 10: Finite size scaling data collapsing along the path of constant $k_B T/J_{NN} = 0.7$ for root-mean-square order parameter and its susceptibility, respectively. $h' = |1 - \frac{H}{H_c}|$ and $h = (1 - \frac{H}{H_c})$. Data are for: $L=32$, \triangleleft ; $L=64$, \blacktriangleright ; $L=128$, \triangleright ; $L=256$, \blacktriangleleft .

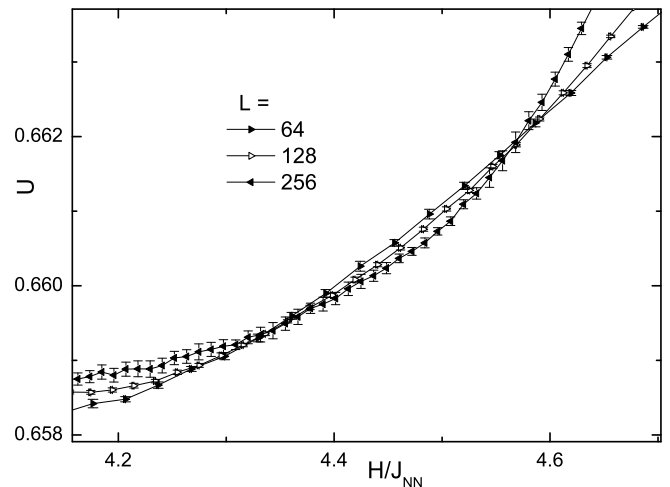


FIG. 11: Fourth order cumulant U versus field H along the path of constant $k_B T/J_{NN} = 0.45$ for lattice size $L = 64, 128, 256$.

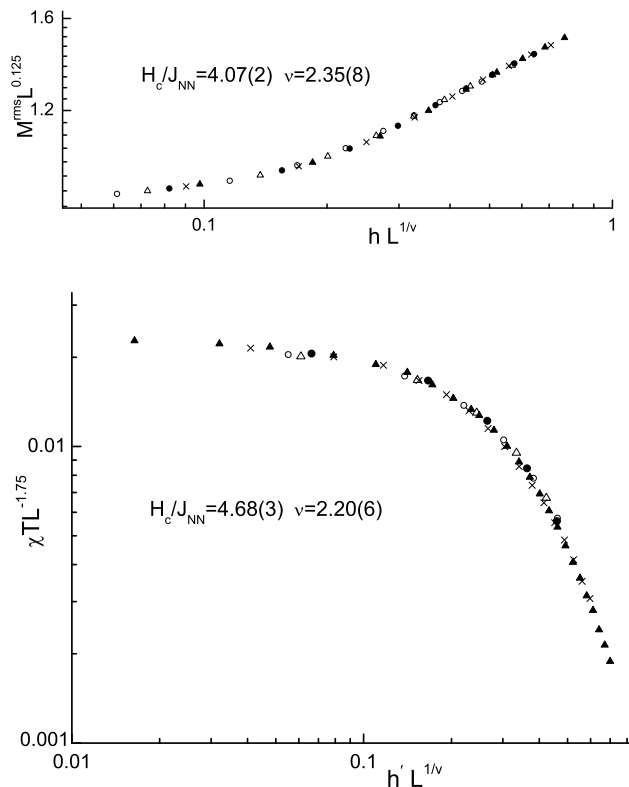


FIG. 12: Finite size scaling data collapsing along paths of constant $k_B T/J_{NN} = 0.5$ for root-mean-square order parameter and its susceptibility, respectively. Data are for: $L=80$, \circ ; $L=100$, Δ ; $L=120$, \bullet ; $L=160$, \times ; $L=200$ \blacktriangle .

not yield any hint of such a bicritical point; but the lack of data points for $T < 0.2$ in Fig.2 precludes us from making a definitive statement about this issue. (Moreover, the reentrant behavior of the (2×1) phase makes it very difficult to study the approach to $T = 0$.)

The variation of the critical exponents is consistent with the changing magnetic field producing different effective anisotropies which, in turn, is expected to yield non-universal behavior[23]. Due to the large values of ν near the bicritical point (and correspondingly strongly negative values of α), we consider it also extremely unlikely that tricritical points could be found along these transition lines as T becomes small.

IV. CONCLUSION

We have carried out large-scale Monte Carlo simulations for the square-lattice Ising model with repulsive (antiferromagnetic) nearest- and next-nearest-neighbor interactions. From the finite size scaling analysis, both transitions from (2×1) and row-shifted (2×2) ordered states to disordered states turn out to be continuous and non-universal. The reentrance behavior of the (2×1) transition line is confirmed, and the proximity to the transition line to the (2×2) state makes it difficult to untangle the low temperature behavior unless quite large lattices are used. It was only possible to obtain the precise, large lattice data needed though the use of GPU computing. No evidence for XY-like behavior is found, and we conclude that there is probably a zero temperature bicritical point. Although the exponent ν varies along the transition line, the exponent ratio β/ν and γ/ν seem to agree with that of the 2D Ising universality class.

Acknowledgements: We would like to thank K. Binder and S.-H. Tsai for illuminating discussions and comments and also T. Preis for introducing us to the use of GPU's for our calculations. Numerical computations have been performed partly at the Research Computing Center of the University of Georgia. This work was supported by NSF grant DMR-0810223.

-
- [1] E. Domany, M. Schick, J.S. Walker, and R.B. Griffiths, Phys. Rev. B **18**, 2209 (1978).
[2] D.P. Landau, Phys. Rev. B **27**, 5604 (1983).
[3] D.P. Landau, J. Appl. Phys. **42**, 1284 (1971).
[4] D.P. Landau, Phys. Rev. B **21**, 1285 (1980).
[5] K. Binder and D.P. Landau, Phys. Rev. B **21**, 1941 (1980).
[6] P.A. Slotte, J. Phys. C **16**, 2935 (1983).
[7] K. Kaski, W. Kinzel, and J.D. Gunton, Phys. Rev. B **27**, 6777 (1983).
[8] J. Amar, K. Kaski, and J.D. Gunton, Phys. Rev. B **29**, 1462 (1984).
[9] J.L. Moran-Lopez, F. Aguilera-Granja, J.M. Sanchez, Phys. Rev. B **48**, 3519 (1993).
[10] J.L. Moran-Lopez, F. Aguilera-Granja, J.M. Sanchez, J. Phys. C **6**, 9759 (1994).
[11] A. Malakis, P. Kalozoumis, and N. Tyraskis, Eur. Phys. J. B **50**, 63 (2006).
[12] F. Wang and D. P. Landau, Phys. Rev. Lett. **86**, 2050 (2001); Phys. Rev. E **64**, 056101 (2001); Comput. Phys. Commun. **147**, 674 (2002).
[13] R.H. Swendsen and J.S. Wang, Phys. Rev. Lett **57**, 2607 (1986).
[14] K. Hukushima and K. Nemoto, J. Phys. Soc. Japan **65**, 1604 (1996).
[15] D.A. Kofke, J. Chem. Phys. **120**, 10852 (2004).
[16] F. James, Comp. Phys. Comm. **60**, 329 (1990).
[17] P. L'Ecuyer, Commun. ACM. **31**, 742 (1988).
[18] M. Matsumoto and T. Nishimura, ACM Trans. on Modeling and Computer Simulation **8**, 3 (1998).
[19] Alan M. Ferrenberg and D.P. Landau, Phys. Rev. B **44**, 5081 (1991).
[20] J. Yang, Y. Wang, and Y. Chen, J. Comp. Phys. **221**, 799 (2007).
[21] J.A. Anderson, C.D. Lorenz, and A. Travesset, J. Comp. Phys. **227**, 5342 (2008).
[22] T. Preis, P. Virnau, W. Paul, and J.J. Schneider, J. Comp. Phys. **228**, 4468 (2009).

[23] G.Y. Hu and S.C. Ying, *Physica* **140A**, 585 (1987).